JOURNAL OF AIRCRAFT
Vol. 31, No. 1, Jan.–Feb. 1994

Sonic Boom Predictions Using a Solution-Adaptive Full-Potential Code

Michael D. Madson*
NASA Ames Research Center, Moffett Field, California 94035

The TranAir full-potential code, which utilizes a solution-adaptive, unstructured Cartesian grid, was used to compute near-field pressure signatures of three generic geometries: 1) a cone-cylinder, 2) a low aspect ratio rectangular wing, and 3) a delta-wing/body. Pressure signatures computed by TranAir are extrapolated to near- and midfield distances using a quasilinear extrapolation technique. Results are compared with wind-tunnel data and, where possible, with extrapolated wind-tunnel data and Whitham-method results. In general, extrapolated TranAir data is in good agreement with experimental and Whitham-method pressure signatures, but peak pressures are slightly underpredicted. It is felt that data computed too close to the model caused some of the discrepancies. Flowfield grid structure was also found to be an important issue in obtaining accurate off-body data. Results were encouraging enough to proceed with the application of TranAir to conceptual configurations in support of the NASA high speed research program (HSRP).

Nomenclature

C_L = lift coefficient
h = distance below model
L = length of model
M_∞ = freestream Mach number
p_{local} = local static pressure
p_∞ = freestream static pressure
x, y, z = Cartesian coordinates
α = angle of attack, deg
Δ_p = $p_{\text{local}} - p_\infty$

Introduction

A RENEWED effort is underway to design a supersonic commercial transport aircraft that has acceptable performance, acceptable emission levels and, if possible, sonic boom noise levels that will allow supersonic overland flight. Existing laws in effect over most of the world prohibit commercial aircraft from flying supersonically over land. It is possible, however, that these laws could be changed if acceptably low sonic boom levels on the ground could be attained. The definition of what constitutes an "acceptable" sonic boom level has yet to be determined, although research in this area is progressing with some success.

The NASA high speed research program (HSRP) has the goal of developing technologies for supersonic commercial transports with acceptable aerodynamic performance and low sonic boom levels on the ground. To assess one of the tools available for designing this airplane, sonic boom calculations were made using the TranAir full-potential code.[1,2] TranAir has successfully computed the aerodynamics of a wide range of complex aircraft geometries.[3–9] This was the first application of a three-dimensional full-potential code to sonic boom prediction. TranAir uses a solution-adaptive unstructured Cartesian grid, which is valuable for computing flows away from the aircraft surface. It can maintain locally dense grids away from the model in regions where flow gradients remain large.

Three generic models were analyzed using TranAir at supersonic Mach numbers: 1) a cone-cylinder, 2) a low aspect ratio rectangular wing, and 3) a delta-wing/body. These configurations were tested in the early 1970s for the purpose of validating extrapolations based on the Whitham theory. The cone-cylinder and rectangular wing were tested at zero angle of attack,[10] and the wing/body model was tested at both zero and positive angles of attack.[11] In some cases, extrapolated experimental data and/or Whitham-method results were also available. Results from these tests verified the validity of extrapolating data measured as close as one body length from the model to cruise altitudes. These geometries have also been recently used to investigate the sonic boom prediction capabilities of both Euler[12] and Navier-Stokes[13] codes.

There remains an issue as to how close to a model pressure-signatures may be measured or computed and still obtain accurate extrapolations to cruise altitude. Pressure signatures were computed by TranAir relatively close to the model (one body length away or less), and were extrapolated to experimental distances using a quasilinear extrapolation technique.[14] TranAir results for the three models serve to validate the use of the code for sonic boom prediction. The results also identify areas where improved results might be obtained by modifying the approach to setting up the computational problem.

Discussion of Method

TranAir solves the nonlinear full-potential equation for subsonic, transonic, and supersonic flow about arbitrary configurations. The theoretical aspects and solution method used by TranAir have been reported[1] and will not be addressed here. Instead, a description of the code from an applications standpoint is presented.

The surface of the configuration is defined by networks of surface panels, in the same manner as panel method codes. This type of surface definition allows for the relatively simple definition of realistic aircraft components such as nacelles, pylons, empennages, external stores, winglets, and other components typically found on commercial, private, and military aircraft. The flowfield is defined by a rectangular array of Cartesian grid points. An example of the surface-paneled delta-wing/body embedded in a uniform Cartesian grid is presented in Fig. 1. The grid need only be large enough to encompass any supercritical flow regions. For supersonic freestream

Received Dec. 9, 1991; revision received April 24, 1992; accepted for publication Oct. 30, 1992.

*Research Engineer, Advanced Aerodynamic Concepts Branch, Aerodynamics Division. Member AIAA.

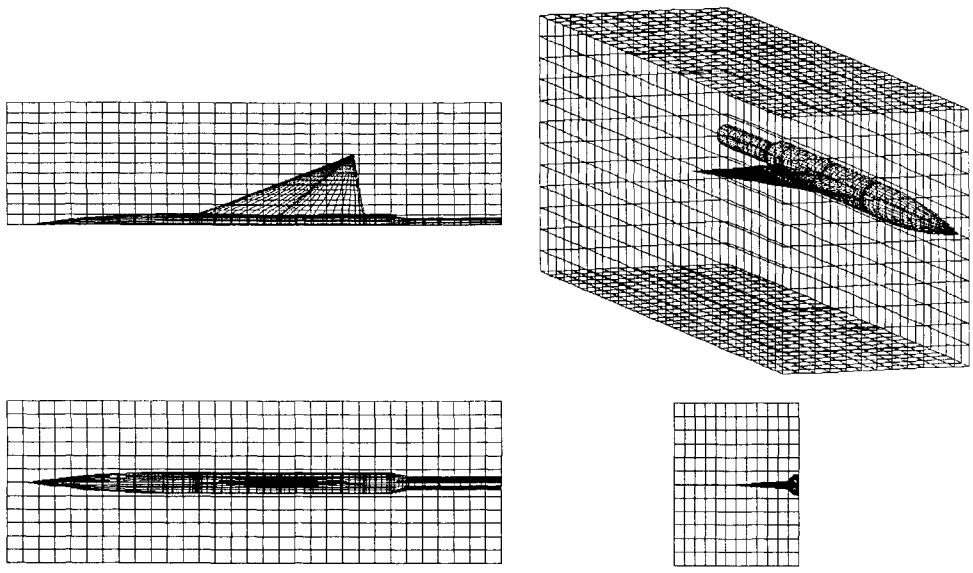

Fig. 1 Surface-paneled delta-wing/body embedded in uniform grid.

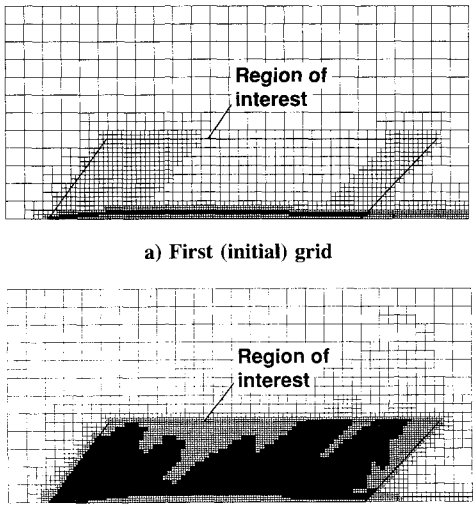

a) First (initial) grid

b) Fourth (final) grid

Fig. 2 Example of solution-adaptive flowfield grid refinements for delta-wing/body.

problems, the grid must extend far enough away that shocks reflected from the grid boundaries do not intersect the configuration surface. These methods of surface grid and flowfield grid definition avoid the use of surface-conforming flowfield grids, and allow for the routine analysis of arbitrary and complex aerodynamic configurations.

The initially uniform flowfield grid is adaptively refined based on local flow conditions. In regions where shocks and large velocity gradients exist, the grid will be refined until adequate resolution is obtained. A refinement consists of dividing a grid box into eight geometrically similar boxes. An oct-tree data structure is used to efficiently store and access pertinent information regarding the refined grid. The user may exert significant influence on the refinement process. One or more hexahedral volumes may be defined by the user within which refinement limits are specified. This volume defines a "region of interest" or "disinterest," depending on whether the user specifies additional refinement or limits the refinement within the volume. Examples of a region of interest include 1) a region enclosing a wing leading edge to increase grid resolution for a careful drag study; and 2) a region enclosing the empennage limiting the refinement so that more grid points are available for a wing/nacelle integration study. Figure 2 provides an example of solution-adaptive grid refinement for the delta-wing/body. The grid slices are along the centerline of the model. The boundary of the region of interest is evident, as is its effect on the refinement process.

Flow quantities are available both on the surface and in the flowfield. A graphics program has been written[2] that allows for inspection of the unstructured grids generated by TranAir. Quantities on the surface may be investigated using the PLOT3D[15] graphics package.

Description of Models

Cone-Cylinder

A drawing of the cone-cylinder[10] is presented in Fig. 3. The cone is 8.6 in. long, and has an included angle of 6.48 deg. The cylinder (sting) is defined back to $x = 15.7$ in. The model is axisymmetric and was tested at $\alpha = 0$ deg, so only one-quarter of the geometry was modeled for the TranAir surface definition. The quarter-cone is defined by 29 panels in the streamwise direction and 9 panels circumferentially. The quarter-cylinder is defined by 17 panels in the streamwise direction and 9 panels circumferentially.

Low Aspect Ratio Rectangular Wing

A drawing of the rectangular wing[10] is provided in Fig. 4. The model consists of a rectangular wing with a chord of 2 in., an aspect ratio of 0.5, and a 0.125-in.-diam sting attached to the trailing edge. The airfoil section is biconvex, with the thickness distribution given in Fig. 4. The geometry is symmetric about the x-y and x-z planes, and was tested at $\alpha = 0$ deg, so one-quarter of the rectangular wing was modeled for TranAir. The wing is defined by 40 panels in the chordwise direction and 8 panels spanwise. The sting is defined to $x = 4$ in. by 12 streamwise panels and 4 circumferential panels.

Delta-Wing/Body

Figure 5 provides a drawing of the delta-wing/body.[11] The wing leading edge is swept back 69 deg, and the trailing edge is swept forward 10 deg. The airfoil section is a 5%-thick double-wedge. Like the two previous models, the wing/body geometry is symmetric about the x-y and x-z planes of symmetry. Experimental data for this configuration are available for both lifting and nonlifting cases, so two TranAir models were defined. For the nonlifting case, the model consists of one-quarter of the geometry. The fuselage is defined by 56 panels streamwise and 9 panels circumferentially. The wing

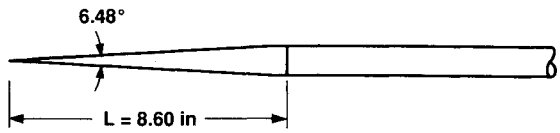

Fig. 3 Cone-cylinder geometry.

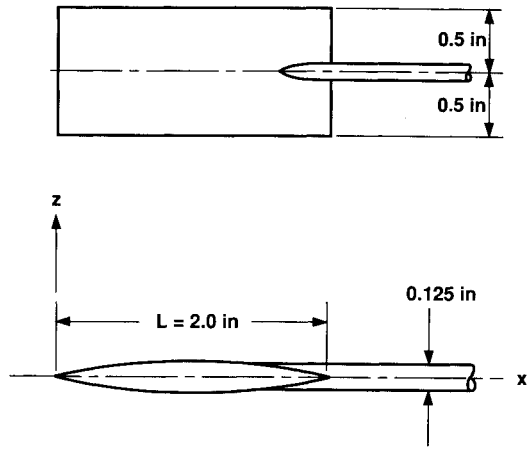

Fig. 4 Low aspect ratio rectangular wing geometry. Thickness distribution is given by $z = (\pi/12.5)[x - (x^2/2)]$.

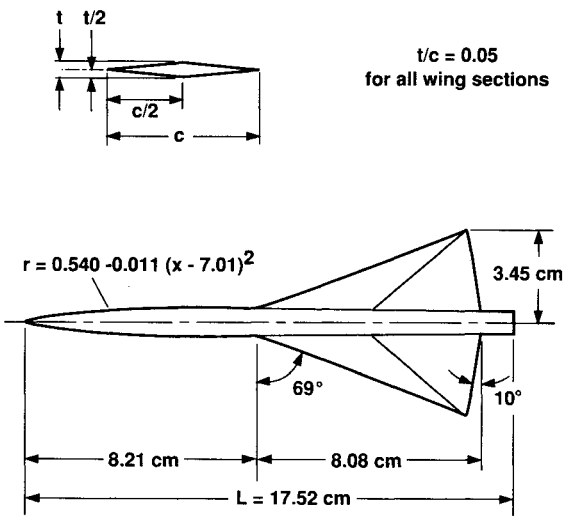

Fig. 5 Delta-wing/body geometry.

consists of 28 panels in the chordwise direction and 17 panels spanwise. The sting section is defined by 10 panels streamwise and 9 panels circumferentially. An expansion ramp connecting the aft end of the fuselage to a 0.3-in.-diam sting is modeled with 6 streamwise panels and 9 circumferential panels. The ramp has a 12-deg expansion angle as suggested by Whitham,[16] and is an approximation of the separated zone at the base of the fuselage. For the lifting case, the lower quarter of the right side of the model was added to the paneled definition using the same distribution as the upper quarter.

Results

All cases took approximately 1.5–2.5 h of CPU time on a Cray Y-MP. This run time includes 1) input processing, 2) construction of multiple solution-adaptive grids, 3) computation of the solution on each of the grids, and 4) postprocessing of the flowfield quantities into aerodynamic coefficients. All cases were run with 4MW of central memory. Each case defined one or more regions of interest to maintain the desired grid density away from the model to more accurately compute off-body flow quantities. Without these regions, the flowfield grid tends to coarsen nearer to the model than is desirable for predicting off-body flow data.

All pressure signature plots presented show values of $\Delta p/p_\infty$ plotted vs x/L. Computational data is shifted along the x axis where necessary to align the plots with experimental data. The alignment is keyed to a distinct flow variable such as maximum pressure. TranAir off-body results are extrapolated to experimental distances using a quasilinear extrapolation technique.[14] The technique is a waveform parameter method based on geometric acoustics for wave amplitude, and isentropic theory for nonlinear wave distortions. Signatures in the wind tunnel are generally measured one or more body lengths from the model. In terms of CPU time and memory requirements, it is difficult to maintain sufficient grid density more than a body length from the model. Computational data generally needs to be extrapolated to experimental distances for comparison. There is an ongoing issue as to how far from the model computational data should be obtained to provide for an accurate extrapolation. This issue is addressed in subsequent sections.

Cone-Cylinder

Experimental data for the cone-cylinder were measured at $M_\infty = 1.68$ and $\alpha = 0$ deg.[10] The uniform global grid consisted of 33, 17, and 17 points in the x, y, and z directions, respectively. The first attempts to compute pressure signatures were made by defining a thin region of interest swept at the Mach angle and running along the centerline for the length of the model. Within this region, extra refinement was specified to minimize numerical diffusion at the off-body planes from which pressures were computed. A cross-stream cut of the finest grid from an early cone-cylinder run is presented in Fig. 6. This cut lies at the longitudinal station where the cone and the cylinder intersect. The cross section of the model, off-body planes at $h/L = 0.25$ and 1, and the region of interest are evident in the figure. The flowfield for this nonlifting case should be axisymmetric, but the asymmetry of the grid yields a nonaxisymmetric flowfield. The plot of surface Mach numbers along several radial stations in Fig. 7 reflects the asymmetry of the solution. A modified region of interest was defined in which a more uniform grid distribution around the model was assured. A cross-stream cut of this modified grid at the cone-cylinder intersection (similar to Fig. 6) is provided

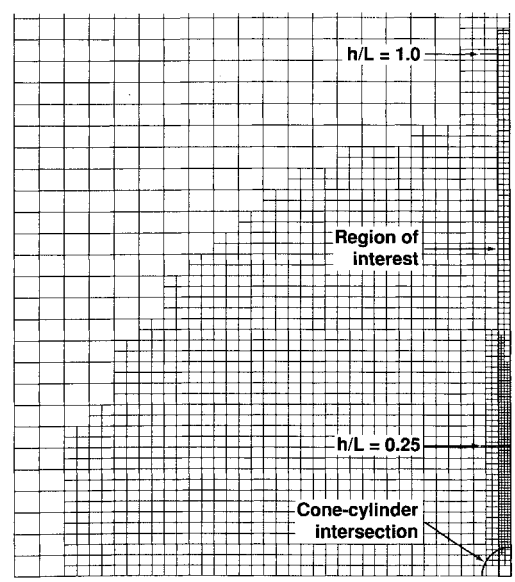

Fig. 6 Cross stream cut from finest grid for cone-cylinder, original grid definition, $M_\infty = 1.68$, $C_L = 0$.

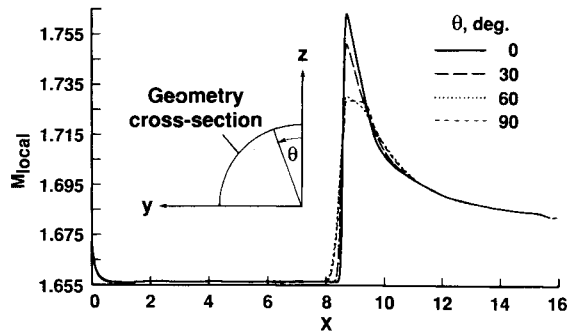

Fig. 7 Surface Mach numbers for cone-cylinder, original grid definition, $M_\infty = 1.68$, $C_L = 0$.

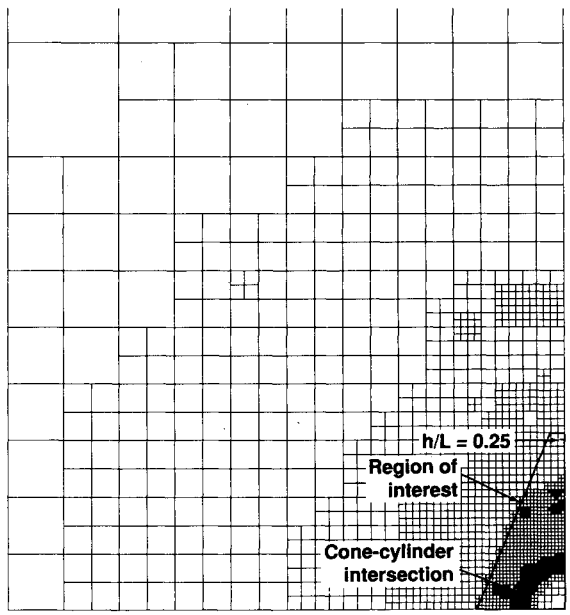

Fig. 8 Cross stream cut from finest grid for cone-cylinder, modified grid definition, $M_\infty = 1.68$, $C_L = 0$.

in Fig. 8. Axisymmetric flow conditions were achieved on the body for this case.

The paneled definition of the cone-cylinder embedded in the finest modified grid is shown in Fig. 9. The figure also shows the user-defined region of interest, and an off-body plane at $h/L = 0.25$, at which TranAir pressure coefficients were computed. The initial pressure signatures computed at $h/L = 1$ were poor, so subsequent attempts to compute signatures at that distance were abandoned for this study. The code generated a series of six refined grids for this case, starting with 24,000 boxes and finishing with 377,000 boxes. The total CPU time for the cone-cylinder case was 8450 s. Results for several refinement strategies were computed for this model. The series of grids defined for the modified grid case yielded a more computationally intensive problem than for the other two models, as reflected by the CPU times for the three cases.

Pressure signatures for the cone-cylinder were measured in the wind tunnel, 10 and 20 body lengths from the model. TranAir results for the original and modified grid cases extrapolated from $h/L = 0.25$ to $h/L = 10$ are presented in Fig. 10a and compared with experimental data. The modified grid case, for which a finer grid resolution was maintained over the entire model, as well as into the flowfield, yielded a much better comparison with experimental data. The finite rise was more accurately predicted, as was the expansion fan and the subsequent pressure recovery along the cylinder. The peak pressure was the same for both cases, which was slightly lower than the measured data. These results demonstrate the importance of an appropriately defined grid in the prediction of off-body pressure signatures.

The extrapolation of TranAir data from $h/L = 0.25$ to $h/L = 20$ for the modified grid case is provided in Fig. 10b. Again, extrapolated TranAir data is in good agreement with experimental data. The underprediction of maximum pressure remained consistent with results at $h/L = 10$. The computed minimum pressure, in good agreement with tunnel data at $h/L = 10$, was overpredicted by 25% vs experiment at $h/L = 20$. The computed data is in good agreement, however, with experimental data extrapolated from $h/L = 10$ to h/L

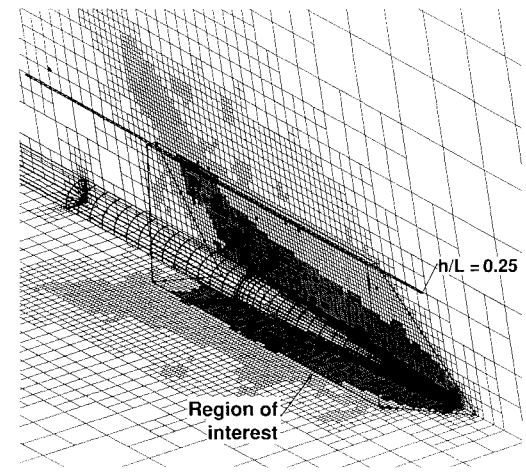

Fig. 9 Cone-cylinder embedded in final solution-adaptive grid, $M_\infty = 1.68$, $C_L = 0$.

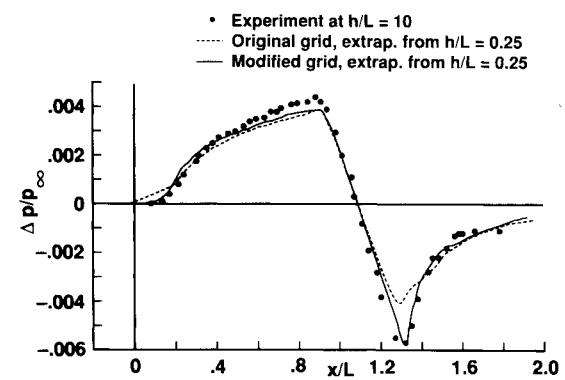

a) $h/L = 10$

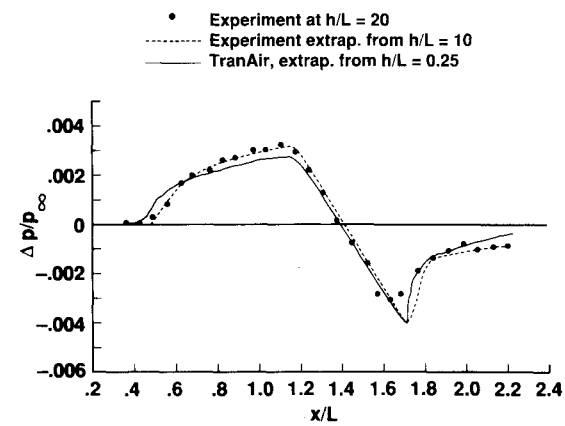

b) $h/L = 20$

Fig. 10 Computational and experimental overpressure predictions for cone-cylinder, $M_\infty = 1.68$, $C_L = 0$.

= 20. A good deal of trust exists in the extrapolation technique because of its successful validation for a wide variety of configurations.[10,11,17] It is not known why the inconsistency in extrapolated and nonextrapolated experimental pressures occurs at $h/L = 20$. It is possible that stream angle and velocity variations existed in the test section of the tunnel where experimental data were measured. Also, experimental data at $h/L = 20$ was obtained from a wind-tunnel model half the length of the model used to measure pressures at $h/L = 10$. It is possible that small geometric differences contributed to the disparity.

Low Aspect Ratio Rectangular Wing

Experimental results for the rectangular wing were measured at $M_\infty = 2.01$ and $\alpha = 0$ deg.[10] The initial uniform grid for TranAir consisted of 41, 9, and 17 points in the x, y, and z directions, respectively. The paneled definition of the wing/sting combination embedded in the finest solution-adaptive grid is shown in Fig. 11. Also seen in the figure are off-body planes at $h/L = 0.25$, 0.5, 0.75, and 1 at which pressure signatures were calculated, and the region of interest defined for the case. Four solution-adaptive grids were generated by TranAir for this case, starting with 24,000 boxes and finishing with 330,000 boxes. The total CPU time for the case was 4246 s.

Experimental data for the rectangular wing were measured one body length from the model. Signatures computed less than one body length from the model were extrapolated to $h/L = 1$. These results, along with experimental data at $h/L = 1$, are shown in Fig. 12. Data extrapolated to $h/L = 1$ improved in comparison with experiment as the distance between the off-body plane and the model increased. This indicates that three-dimensional effects for this case may not be fully captured by the grid in Fig. 11, and data extrapolated from less than one body length away may not be reliable. This is consistent with previous findings from applications of the extrapolation method.[10,11] Nonextrapolated TranAir results at $h/L = 1$ are generally in good agreement with the TranAir data extrapolated from $h/L = 0.75$ and experimental data, although it appears that the grid resolution at $h/L = 1$ may have been too coarse to maintain leading-edge shock strength. The strength of the leading-edge shock is consistently underpredicted by extrapolated and nonextrapolated data. The trailing-edge shock predicted by extrapolated TranAir data is downstream of the experimental shock location, although the magnitude of the pressure is well-predicted. The sting is modeled for the computations, but the solution on the grid in Fig. 11 indicates that the sting effect diminishes rapidly with distance from the model. The aft shock in the TranAir prediction appears to be induced solely by the wing trailing edge. The sting on the wind-tunnel model may have induced a shock upstream of the trailing edge along the centerline. There may also be viscous effects tending to induce a shock upstream of the trailing edge.

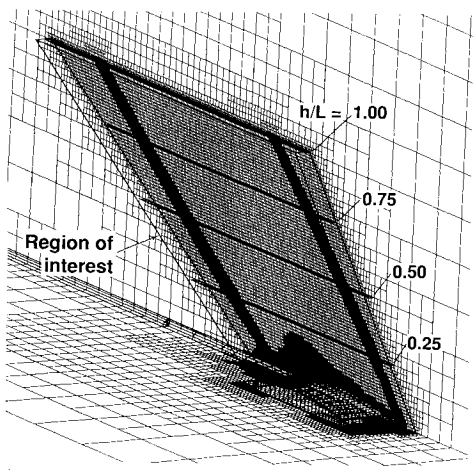

Fig. 11 Rectangular wing embedded in final solution-adaptive grid, $M_\infty = 2.01$, $C_L = 0$.

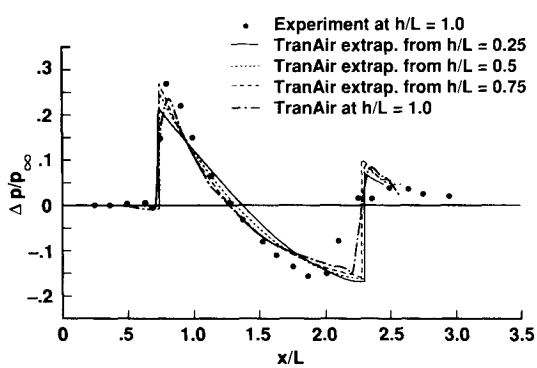

Fig. 12 Computational and experimental overpressure predictions for rectangular wing, $M_\infty = 2.01$, $C_L = 0$, $h/L = 1$.

Delta-Wing/Body

Experimental results for the delta-wing/body are available at $M_\infty = 1.68$ and 2.7 for both lifting and nonlifting cases.[11] This section compares TranAir results with experiment at $M_\infty = 1.68$ for lifting and nonlifting cases. The uniform global grid for the wing/body case consisted of 49, 13, and 17 points in the x, y, and z directions, respectively. The paneled definition of the delta-wing/body embedded in the finest of the solution-adaptive grids for the nonlifting case is shown in Fig. 13. Also seen in the figure is the region of interest defined for the problem and the planes at $h/L = 0.1$, 0.2, and 0.325 at which TranAir results were computed. The sequence of grids generated during this run consisted of 25,000, 62,000, 140,000, and 330,000 grid boxes, respectively. The total CPU time for the delta-wing/body case was 5000 s. Pressure signatures for this model were measured in the wind tunnel at $h/L = 3.6$. Experimental data extrapolated to $h/L = 130$ are available, as are Whitham-method[16] predictions.

An experiment/TranAir correlation for $C_L = 0$ at $h/L = 3.6$ is presented in Fig. 14a. The nose shock extrapolated from TranAir data at $h/L = 0.1$ and 0.2 is in good agreement with experiment. TranAir data extrapolated from $h/L = 0.325$ slightly underpredicts the nose shock. The wing leading-edge shock is significantly underpredicted by extrapolations from all three off-body planes. As the distance from the model increases, the extrapolated expansion and shock from the wing trailing edge and fuselage base improves in comparison

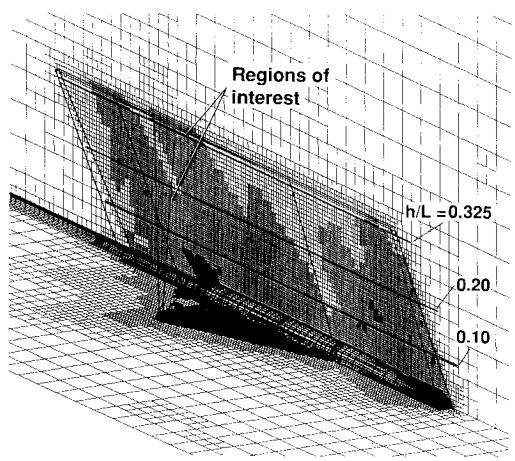

Fig. 13 Delta-wing/body embedded in final solution-adaptive grid, $M_\infty = 1.68$, $C_L = 0$.

with experiment. Two regions of interest were defined that attempted to maintain adequate grid resolution along the centerline, and to accurately capture three-dimensional effects to $h/L = 0.325$. It is possible that the regions defined were not effective in completely capturing three-dimensional effects, particularly near the wing leading edge. Results from the rectangular wing indicate that off-body planes defined for the wing/body may be too close to allow for an accurate extrapolation. Despite the poor leading-edge shock prediction, TranAir data extrapolated from $h/L = 0.325$ to $h/L = 130$ is in reasonable agreement with extrapolated experimental data and the Whitham theory as seen in Fig. 14b. The location of the middle shock is slightly downstream because of the weakness of the wing leading-edge shock computed in the near field. Data extrapolated from the two closest planes (not shown in Fig. 14b) were in poor agreement with extrapolated experimental data and the Whitham theory. This is consistent with the knowledge that inaccurate extrapolations are obtained from data measured too close to the body.

Similar results are observed for $C_L = 0.08$, shown in Fig. 15. Comparisons with experiment are similar to those for the nonlifting case. The significant difference at $C_L = 0.08$ is that the wing leading-edge shock is in much better agreement with experiment than it was at $C_L = 0$. The main difference between the two cases is the absence of an x-y symmetry plane for the lifting case. It is felt that this difference affected the accuracy of the wing leading-edge shock prediction for the nonlifting case. It may also explain the difficulty in obtaining the correct leading-edge shock strength for the rectangular wing.

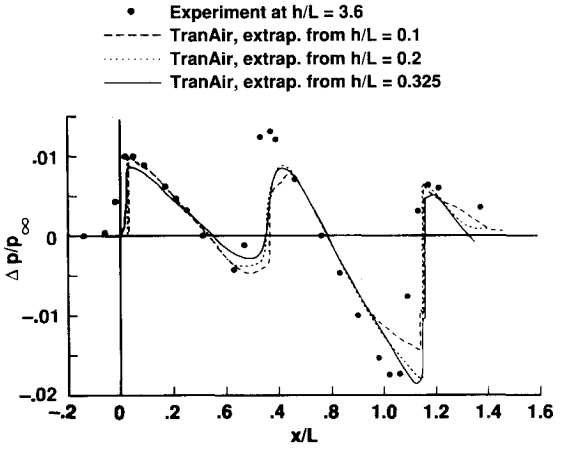

a) $h/L = 3.6$

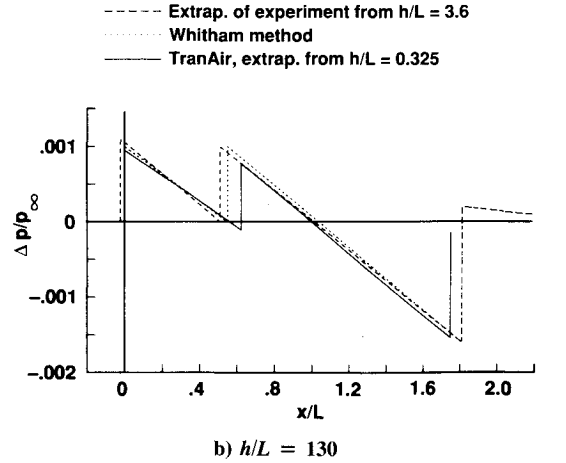

b) $h/L = 130$

Fig. 14 Computational, experimental, and theoretical overpressure predictions for delta-wing/body, $M_\infty = 1.68$, $C_L = 0$.

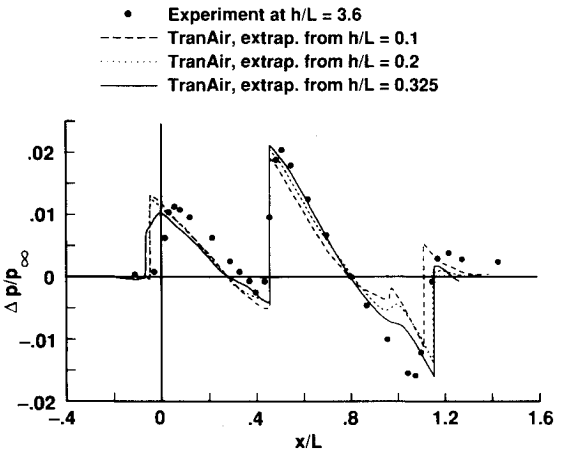

a) $h/L = 3.6$

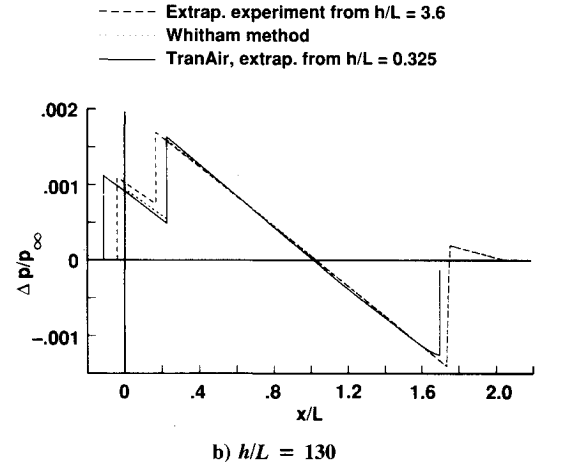

b) $h/L = 130$

Fig. 15 Computational, experimental, and theoretical overpressure predictions for delta-wing/body, $M_\infty = 1.68$, $C_L = 0.08$.

The discontinuity in the extrapolated TranAir pressure signature near $x/L = 0.95$ (Fig. 15a) is the wing trailing-edge shock, interrupted by the expansion along the 12-deg ramp, followed by the shock at the ramp/sting intersection. A discussion of the base/sting model appears in the modeling section, and can be seen in Figs. 1 and 13. The effect of the base/sting model is also evident in Fig. 14a for $C_L = 0$. The increased strength of the trailing-edge shock and sting shock overshadows the expansion from the fuselage base to the sting. The signature extrapolated from $h/L = 0.325$ to $h/L = 130$ closely agrees with extrapolated experimental data and the Whitham theory as shown in Fig. 15b. Data extrapolated from the two closest planes (not shown in Fig. 15b) were again in poor agreement.

Conclusions

In general, extrapolated TranAir pressure signatures compare favorably with experimental and Whitham-method results at near- and midfield locations. There were indications that some TranAir results were computed too near to the models to obtain accurate extrapolations. Computation of accurate near-field pressure signatures requires a flowfield grid that is dense enough to accurately predict the flowfield away from the model. It is also necessary to extract computational pressure signatures far enough from the model to ensure that all three-dimensional effects have reached the centerline. Three-dimensional effects may be significant to one or more body lengths from the model, depending on model geometry. Accurate near-field predictions are necessary to accurately extrapolate signatures to mid- and far-field distances. TranAir is capable of more accurate near-field pre-

dictions by improving the definition of the regions of interest for each case. The solution-adaptive capability allows for this type of grid modification with little difficulty. Further research is recommended to determine the best grid structure for computing near-field pressure signatures.

The ability of TranAir to routinely model and compute flows about arbitrary configurations using a solution-adaptive grid strategy makes it valuable for rapid sonic boom analysis of realistic configurations. TranAir is currently being used to predict the pressure signatures and aerodynamic performance of conceptual configurations in support of the HSRP.

References

[1]Johnson, F. T., Samant, S. S., Bieterman, M. B., Melvin, R. G., Young, D. P., Bussoletti, J. E., and Hilmes, C. L., "TRANAIR: A Full-Potential, Solution-Adaptive Rectangular Grid Code for Predicting Subsonic, Transonic, and Supersonic Flows About Arbitrary Configurations (Theory Document)," NASA CR-4348, Dec. 1992.

[2]Johnson, F. T., Samant, S. S., Bieterman, M. B., Melvin, R. G., Young, D. P., Bussoletti, J. E., and Hilmes, C. L., "TRANAIR: A Full-Potential, Solution-Adaptive Rectangular Grid Code for Predicting Subsonic, Transonic, and Supersonic Flows About Arbitrary Configurations (User Guide)," NASA CR-4349, Dec. 1992.

[3]Madson, M. D., "Transonic Analysis of the F-16A with Under-Wing Fuel Tanks: An Application of the TranAir Full-Potential Code," AIAA Paper 87-1198, June 1987.

[4]Madson, M. D., Carmichael, R. L., and Mendoza, J. P., "Aerodynamic Analysis of Three Advanced Configurations Using the TranAir Full-Potential Code," NASA CP-3020, Vol. 1, Pt. 2, 1989, pp. 437–452.

[5]Goodsell, A. M., Madson, M. D., and Melton, J. E., "TranAir and Euler Computations of a Generic Fighter Including Comparisons with Experimental Data," AIAA Paper 89-0263, Jan. 1989.

[6]Johnson, F. T., Samant, S. S., Bieterman, M. B., Melvin, R. G., Young, D. P., Bussoletti, J. E., and Madson, M. D., "Application of the TranAir Rectangular Grid Approach to the Aerodynamic Analysis of Complex Configurations," *Proceedings on Applications of Mesh Generation to Complex 3-D Configurations*, AGARD CP-464, March 1990, pp. 21-1–21-12.

[7]Chen, A. W., Curtin, M. M., Carlson, R. B., and Tinoco, E. N., "TRANAIR Applications to Engine/Airframe Integration," *Journal of Aircraft*, Vol. 27, No. 8, pp. 716–721.

[8]Cenko, A., Tseng, W., Phillips, K., and Madson, M., "TranAir Applications to Transonic Flowfield Predictions," AIAA Paper 91-0201, Jan. 1991.

[9]Madson, M. D., and Erickson, L. L., "Toward the Routine Aerodynamic Analysis of Complex Configurations," *Applied Computational Aerodynamics*, Vol. 125, Progress in Astronautics and Aeronautics, AIAA, Washington, DC, 1990.

[10]Mendoza, J. P., and Hicks, R. M., "Further Studies of the Extrapolation of Near-Field Overpressure Data," NASA TM-X-2219, March 1971.

[11]Hunton, L. W., Hicks, R. M., and Mendoza, J. P., "Some Effects of Wing Planform on Sonic Boom," NASA TN-D-7160, Jan. 1973.

[12]Cliff, S. E., and Thomas, S. D., "Euler/Experiment Correlations of Sonic Boom Pressure Signatures," AIAA Paper 91-3276, Sept. 1991.

[13]Cheung, S. H., Edwards, T. A., and Lawrence, S. L., "Application of CFD to Sonic Boom Near and Mid Flow-Field Prediction," AIAA Paper 90-3999, Oct. 1990.

[14]Thomas, C. L., "Extrapolation of Sonic Boom Pressure Signatures by the Waveform Parameter Method," NASA TN-D-6832, June 1972.

[15]Walatka, P. P., Buning, P. G., Pierce, L., and Elson, P. A., "PLOT3D User's Manual Version 3.6," NASA TM-101067, March 1990.

[16]Whitham, G. B., "The Flow Pattern of a Supersonic Projectile," *Communications on Pure and Applied Mathematics*, Vol. V, No. 3, 1952, pp. 301–348.

[17]Hicks, R. M., and Mendoza, J. P., "Prediction of Aircraft Sonic Boom Characteristics from Experimental Near Field Results," NASA TM-X-1477, Nov. 1967.